Materials Characterization 174 (2021) 110973

Contents lists available at ScienceDirect

Materials Characterization

journal homepage: www.elsevier.com/locate/matchar

Investigation of spatial nano-structure development of the hardened C_3S pastes by serial block-face SEM

Fei Yang [a], Xianping Liu [a,b,*], Peiming Wang [a,b], Shunfeng Wang [a], Ian Robinson [a,c], Bo Chen [a,b,c,*]

[a] School of Materials Science and Engineering, Tongji University, Shanghai 201804, China
[b] Key Laboratory of Advanced Civil Engineering Materials (Tongji University), Ministry of Education, Shanghai 201804, China
[c] London Centre for Nanotechnology, University College London, London WC1H 0AH, UK

ARTICLE INFO

Keywords:
Serial block-face scanning electron microscopy (SBFSEM)
C_3S pastes
Three-dimensional imaging
Degree of hydration
Porosity

ABSTRACT

Hardened tricalcium silicate (C_3S) pastes cured for different times from 12 h to 28 days were studied by serial block-face scanning electron microscopy (SBFSEM) with the region of interest (ROI) of (2.0×10^4) μm^3 and their three-dimensional (3D) spatial structures with a voxel size down to 16.6 nm × 16.6 nm × 20 nm were quantitatively analyzed. From these 3D images, the morphological characteristics of different components of the hardened C_3S pastes in three-dimensions are observed directly, such as the connected pores and closed pores. Additionally, the degree of hydration and porosity of the samples are measured as well. Results show that the evolution of the degree of hydration reveals the high reactivity of C_3S with water. The formation of the pore network is a complex process which includes not only the partition of the open pores but also the continued hydration of C_3S in the closed pores, especially the newly formed closed pores during hydration. The quantitative analysis from SBFSEM measurements were compared with those from traditional TG-DSC and MIP, and it proves that SBFSEM has good applicability in the field of cement-based materials.

1. Introduction

Tricalcium silicate (C_3S) is the most important constituent of the normal Portland cement clinkers and accounts for about 50% - 70% of its weight [1]. The main hydrates produced by the normal Portland cement hydration for strength development are hydrated calcium silicate (C-S-H) and calcium hydroxide (CH), both of them are generated mostly by the reaction of C_3S with water [2]. The structure and hydrates of C_3S are relatively simple compared with those of normal Portland cement, therefore C_3S is often used instead of normal Portland cement for studying the hydration process [3,4]. Since the hydration process and microstructure characteristics determine the properties of the cement mortar and concrete, such as strength development and durability, it has been studied for decades. Therefore, progress made in understanding the microstructure development during cement hydration will attract wide attention, and could help researchers to regulate and control the process, hence improving the quality and decreasing the cost of the cement mortar and concrete [5–7]. However, so far, the mechanism of cement hydration has not yet been fully understood. The microstructure characterization, especially the characterization of pore structure evolution, has not been able to obtain comprehensive results because the limitations of the mainstream measurement methods. In fact, currently, due to the lack of sufficient experimental observation and data analysis, such as the direct observations that could be used to guide and verify the numerical simulation of the microstructure and its development, the proposed mechanism of cement hydration still has not yet reached full consensus [8–11].

Thermal analysis (TA), quantitative X-ray diffraction (QXRD) analysis, mercury intrusion porosimetry (MIP), nitrogen adsorption, small angle scattering (SAS) by X-rays or neutrons, back-scattered electron image analysis (BSE-IA), and X-ray computed tomography (CT), etc. have been used to study the cement hydration and their microstructure development. Among those techniques, TA and QXRD analysis are often used to identify phases and study the hydration degree of cement pastes [7,12]. MIP can measure most of the pores from the nanometer to micrometer level [13]. The nitrogen adsorption method is mainly used to analyze the nano-scale pores [14]. Most of the gel pores and gel particles are mainly characterized by SAS [15]. BSE-IA performs

* Corresponding authors at: School of Materials Science and Engineering, Tongji University, Shanghai 201804, China.
E-mail addresses: lxp@tongji.edu.cn (X. Liu), bo.chen@tongji.edu.cn (B. Chen).

https://doi.org/10.1016/j.matchar.2021.110973
Received 30 October 2020; Received in revised form 10 February 2021; Accepted 12 February 2021
Available online 17 February 2021

statistical analysis on two-dimensional (2D) BSE micrographs, therefore could quantitate the hydration degree and pores of cement-based materials [16]. X-ray CT can perform three-dimensional (3D) structure measurement of the samples based on the acquired 2D projections [17–20]. Among those measurement methods for cement-based materials, each has its advantages and disadvantages. For example, methods for characterizing the pore structure, such as MIP, nitrogen adsorption and SAS are all indirect measurement methods and they are not able to characterize the porosity heterogeneity along the altered profile. BSE-IA can be used to calculate the hydration degree and analyze pore structure from the directly-obtained images, but it is limited to two dimensions. X-ray CT can acquire 3D spatial images of the cement pastes features at a micro or sub-micron resolution, such as air-filled voids, pore network, fractures, etc. Besides expectation of continuously improving the spatial resolution of this technology, quantitative analysis of 3D images and regarding with real engineering problems is a new perspective. Compared with the other methods, in the last a couple of decades, 3D visualization techniques have great advantages in revealing the real spatial distribution and irregular morphology of the hardened cement pastes [21].

Serial block-face scanning electron microscopy (SBFSEM) [22] is a 3D imaging technology originally designed for biological and life science research [23] and has been gradually extended to other research fields recently. It is becoming one of the key methods for acquiring 3D images of polymer materials [24], composite materials and metal alloys [25–27]. From those results, the internal features of the measured materials can be observed directly and analyzed quantitatively. For SBFSEM measurements, materials are usually embedded in epoxy resin first, which can effectively avoid the collapse of their 3D structure while doing sectioning-imaging in the vacuum environment of the electron microscopes. The embedded sample block is alternately cut by the built-in ultra-microtome and then imaged. The thickness of the cut slices along the *Z*-axis direction could be 10 nm to 200 nm. The resolution of image slices in the XY plane (the electron microscope imaging plane) can be as high as about 2 nm, depending on the sample and the used electron microscope. Once the sample is cut, the newly exposed surface is imaged by using back-scattered electron detector, and then a new cut would be performed again. This process is automatically performed continuously according to the set parameters [28,29]. The 3D image is then obtained by stacking the serial slice images, automatically registered and in sequence, together.

SBFSEM was used to study the hydration of C_3S with the water to cement ratio (w/c) of 0.6 in this work. In BSE imaging, the grey-scale levels of unhydrated regions of the raw C_3S, hydrates and pores in the hardened C_3S pastes are all different [30]. Based on the resulting grey-scale levels of the slice images, ImageJ [31] and Avizo software were used to perform segmentation, 3D rendering and quantitative analysis on hundreds of slices obtained by SBFSEM [32]. In this research, the hydration degree and pore structure of the hardened C_3S paste hydrated for 7 days obtained by SBFSEM was compared with those obtained by the other methods such as thermogravimetric-differential scanning calorimetry (TG-DSC) and MIP to verify the applicability of the technique. Finally, SBFSEM was used to study the evolution of hydration degree and pore structure of the hardened C_3S pastes after various hydration ages including 12 h, 3 days, 7 days and 28 days.

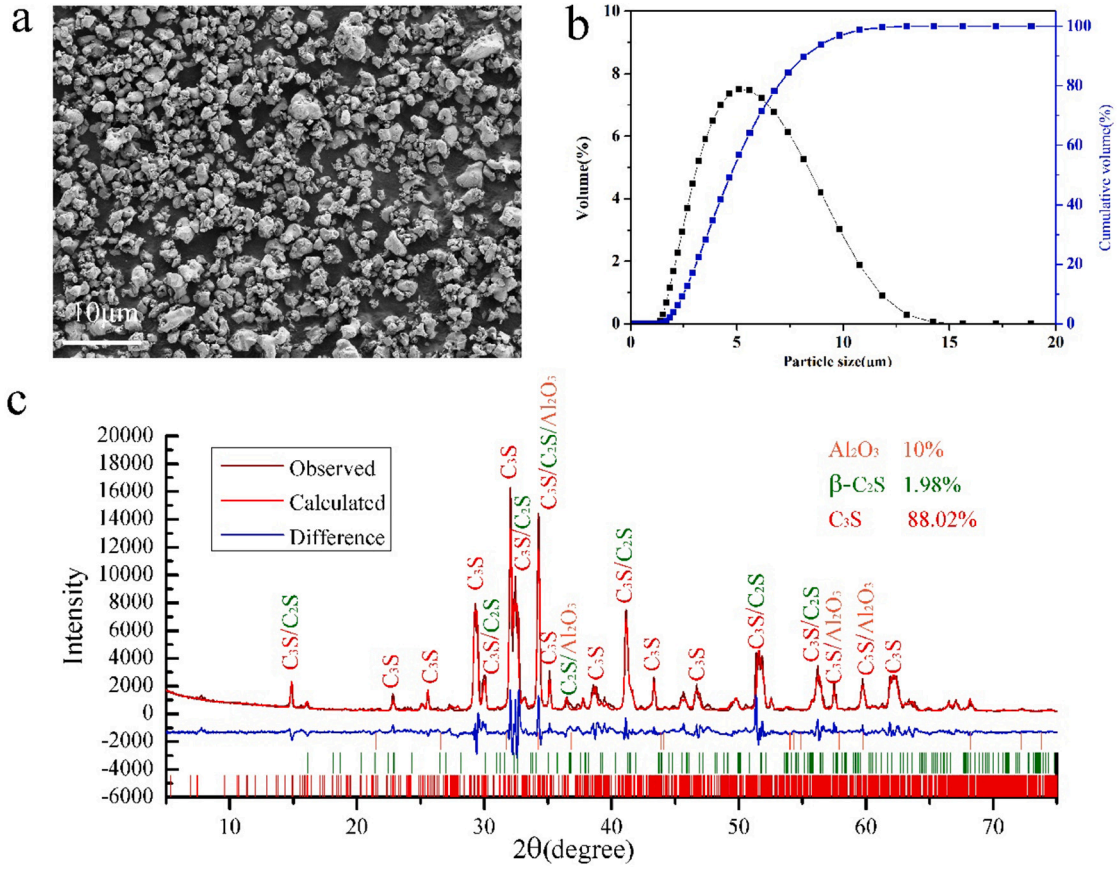

Fig. 1. Characterization of the raw C_3S specimen. (a) Secondary electron micrograph of the C_3S; (b) Particle size distribution of the C_3S; (c) Rietveld refinement result for the mixture of C_3S with 10% Al_2O_3 (using Cu Kα radiation at 40 kV and 250 mA, with 2θ from 5° to 75°, stepping-scan at a step of 0.02° and the exposure time of 2 s, TOPAS V4.2 was used to refine the XRD pattern of the Al_2O_3-C_3S mixer specimen).

2. Materials and methods

2.1. Raw materials and the sample preparation

C_3S used in the work was provided by DMT Materials Technology Co., Ltd. A secondary electron micrograph obtained by a scanning electron microscope (SEM, Sigma 300VP, Carl Zeiss Microscopy GmbH) is presented in Fig. 1a. The morphology of the triclinic C_3S particles look regular. The specific area measured by the Brunauer-Emmett-Teller method (BET, Autosorb-iQ3, Quantachrome Instruments) is (1.8212 ± 0.0028) m^2/g. According to the particle size distribution obtained by a laser particle size analyzer (LPSA, LS230, Beckman Coulter Ltd.) in Fig. 1b, most of the C_3S particles are between 1 μm and 6 μm. In order to evaluate the purity of the raw C_3S, 10% of Al_2O_3 by weight was used as a standard reference to mix with the C_3S for QXRD analysis by an X-ray Diffractometer (XRD, Rigaku D/max 2550 VB3+/PC, Rigaku International Corporation). The Rietveld refinement result presented in Fig. 1c shows that the raw material contains 97.8% of triclinic C_3S and 2.2% of β-C_2S.

Since the C_3S particles are ultra-fine, high w/c of 0.6 in this work is necessary to ensure better homogeneity of the mixed paste. The C_3S particles were mixed with deionized water and stirred quickly with a glass rod for about 3 min. The well mixed paste was then kept in sealed plastic containers for curing of 12 h, 3 days, 7 days and 28 days at the temperature of 20 ± 2 °C. To ensure the hydration of the target samples were completely stopped [33], the cured samples at predetermined ages were broken into pieces smaller than 1 mm, and were then stopped hydration by immersing in the ethanol for 1 day and drying at 40 ± 1 °C in an oven for several days until the samples reached constant weight. These prepared samples were then kept in a vacuum drier for no longer than a couple of days before further processing and measurements.

For measurements by SBFSEM, the above hydration-stopped C_3S paste at various ages are embedded in the epoxy resin in advance. The epoxy resin used in this experiment is Agar 100 resin supplied by Agar Scientific Ltd. The embedment was performed under low vacuum condition with a pressure of 10 kPa, and then the embedded samples were placed at room temperature of about 20 °C for 30 min, followed by keeping at 60 °C for about 48 h for hardening. A microtome (EM UC7, Leica Microsystems Inc.) was used to trim the embedded sample into a pyramid shape, and then a total depth of about 5 μm of the sample was cut by a glass knife to ensure that the upper surface of the C_3S paste to be measured by SBFSEM is flat. Finally, conductive silver paste was applied around the pyramid-shaped sample to help reduce charging on the sample surface during SBFSEM measurements.

For measurement by TG-DSC, the above hydration-stopped C_3S pastes at various ages were ground into fine powder smaller than 5 μm. In order to calculate the degree of hydration of C_3S with TG-DSC, a fully hydrated C_3S paste sample was prepared separately. The already-hardened C_3S paste with w/c of 0.6 at the hydration age of 180 days was broken and ground into powder, and then was mixed with excess water for continual hydration until 360 days. It was finally stopped hydration by immersing in the ethanol for 1 day and drying at 40 ± 1 °C in an oven. After grounding into the fine powder smaller than 5 μm, it was measured by XRD and TG-DSC. The main crystal phase, CH, in the XRD pattern in Fig. 2 confirmed that C_3S was fully hydrated since there were seldom crystal phases from raw materials.

For measurement by MIP, samples of the above hydration-stopped C_3S pastes at various ages were made between 3 mm and 5 mm.

2.2. Methods

The SBFSEM system used in this work consists of an SEM (Sigma 300VP, Carl Zeiss Microscopy GmbH) and a commercial 3View unit (3View®2.XP, Gatan Inc.) [22]. The BSE signal was selected to image the samples in order to show various components in the samples with different grey-scale levels. The 3View unit, a built-in ultra-microtome system of SBFSEM, performs continuous cutting and BSE imaging according to the set parameters. That is, after each automatic cutting, the freshly exposed surface of the sample is imaged by the BSE detector. This serial sectioning and imaging continues until hundreds or thousands of BSE micrographs are acquired upon request [22].

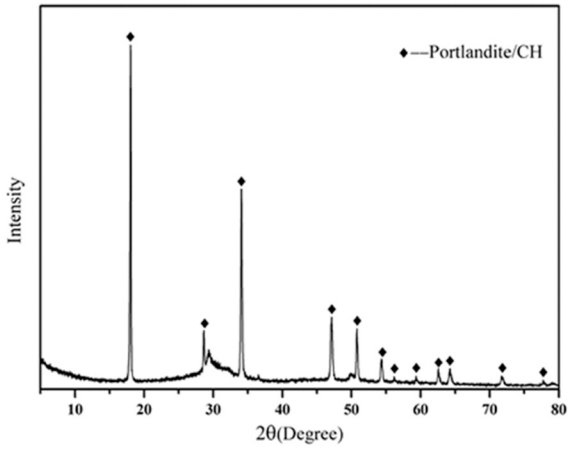

Fig. 2. The XRD pattern of the hardened C_3S paste hydrated for 360 days (using Cu Kα radiation at 40 kV and 250 mA, continuous scan at 5°/min).

In this study, the cutting thickness of each slice and cutting speed of the ultra-microtome were set to be 20 nm and 0.6 mm/s, respectively. The dwell time for the BSE detector was 1.5 μs and the pixel size of the acquired BSE images was 16.6 nm × 16.6 nm, and the SEM was working under an accelerating voltage of 1 keV. Under such parameter setting, a data set consisting of 900 slices were collected in about 8 h.

The TG-DSC curves were acquired by an SDT Q600 analyzer (TA Instrument, USA) at heating rate of 10 °C/min in N_2 flow at a rate of 60 mL/min. CH decomposition was calculated according to the TG measurement result. The TG-DSC result was used to calculate the CH content, and hence quantitate the degree of hydration of the hardened C_3S pastes.

An MIP instrument (Auto pore IV9500 V1.09, Micromeritics Instrument Corp.) was used to measure the pore size distribution of the sample. The penetration pressure was set from 0.1 psi (689.5 Pa) to 33,000 psi (2.275×10^8 Pa). The contacting angle of 140° was used for the calculation of pore size.

2.3. Data processing

Preprocessing of the data was performed by ImageJ [31] before doing segmentation on the images, and then the segmentation and quantitative analysis of the 3D images were done by Avizo [34,35]. According to the BSE image contrast of cement materials [16,30], pores, hydrates and unhydrated C_3S are shown in different grey-scale levels. The tangent method [36,37] is used to make a preliminary determination of the threshold grey-scale levels for different components in the specimens, which provides a basis for subsequent segmentation by Avizo. In detail, the grey-scale threshold values used to identify the hydrates and unhydrated C_3S is corresponding to the transition point T1 in Fig. S1 in the supplementary materials, where a change of the tangent slope of the grey-scale histogram occurs. Voxels with grey-scale values smaller than T1 are hydrates (or pores) and those higher than T1 are unhydrated C_3S. To further determine the preliminary grey-scale threshold value between pores and hydrates, tangent-slope grey-level thresholding method [36,37] was used. The threshold value is corresponding to the grey-scale value at the inflection point T2 in the cumulative volume fraction curve in Fig. S1. As 8 bit data were used, for the specimens analyzed in this work, the primary threshold values to distinguish between pores and hydrates are from 120 to 140, and to distinguish between hydrates and unhydrated C_3S are from 150 to 170.

The used exact values vary a bit while the specimens are different. The further minor adjustment on the grey-scale threshold values used for the segmentation of 3D images by Avizo are performed manually under help by naked eyes. Data processing by Avizo mainly includes the following steps: alignment, noise reduction, segmentation, visualization and volume analysis. The main data processing flow is shown in Fig. S2 in the supplementary materials.

3. Results and discussion

3.1. SBFSEM imaging

Fig. 3 shows the two-dimensional (2D) slice images of the hardened C_3S paste after 7 days of hydration from SBFSEM measurement. Fig. 3a is the BSE image of the cross-section of the whole mounted sample at lower magnification. The grey part in the middle is identified as the hardened C_3S paste, the surrounding large darker region is the epoxy resin, and the regions with white dots around the edges of the epoxy resin is the conductive silver paste. Only the central part of the sample, i.e. the hardened C_3S paste, was chosen for high-resolution imaging. Fig. 3b shows the first acquired two-dimensional (2D) BSE image of the serial slices of the hardened C_3S paste after 7 days of hydration. The generated pixel size of the image is 16.6 nm × 16.6 nm. The black parts in Fig. 3b represent the pores, the large grey part is the hydrates, and the whiter parts are unhydrated C_3S particles. Fig. 3c shows the 100th, 300th, 500th and 700th images in the serial of slice images obtained by SBFSEM, the changes at the corresponding positions in different images can also be clearly seen.

Region of interest (ROI) of about 2.0 × 10^4 μm^3 (18 μm × 33 μm × 33 μm) was chosen from the central region of the embedded hardened C_3S paste in this work for 3D rendering and analysis (see details in 3.2.3). Fig. 4 shows the 3D rendered volume images of the hardened C_3S paste after 12 h (Fig.s 4a-c), 3 days (Fig.s 4d-f), 7 days (Fig.s 4 g-i) and 28 days (Fig.s 4j-l) of hydration, respectively, in which the blue parts represent the unhydrated C_3S particles, the red and yellow parts represent the pores and the grey regions are the hydrates. The distributions of the unhydrated C_3S and the tortuosity and connectivity of the 3D pore network within the specimens after 12 h (Fig.s 4b and c), 3 days (Fig.s 4e and f), 7 days (Fig.s 4 h and i) and 28 days (Fig.s 4 k and l) of hydration are also visualized clearly in Fig. 4.

3.2. Quantitative characterization by SBFSEM

From those segmented 3D images in Fig. 4, the degree of hydration and the porosity of the measured specimens can be calculated using Avizo software.

3.2.1. Degree of hydration

Based on the 3D analysis, the degree of hydration at time t can be calculated according to the Eqs. (1) and (2) [38,39], which results in 55.6%, 81.3% and 88.8% at 12 h, 7 days and 28 days of hydration. The evolution of the degree of hydration at various ages is shown in Fig. 5a.

$$\alpha_t(\%) = \left\{1 - \frac{V(t)}{V(0)}\right\} \times 100\% \quad (1)$$

$$V(0)(\%) = \frac{1}{1 + \rho_c \times (m_w/m_c)} \times 100\% \quad (2)$$

In the Eqs. (1) and (2), α_t presents the degree of hydration of the C_3S; $V(t)$ presents the volume of the unhydrated C_3S at the hydration time t, which can be derived from the 3D analysis of the volume images. $V(0)$ presents the volume of the C_3S before hydration; ρ_c presents the specific gravity of C_3S, which is 3.1. It is measured by helium pycnometry. m_w and m_c presents the mass of water and C_3S involved in the hydration respectively, and m_w/m_c (w/c) is 0.6.

3.2.2. Porosity

The porosity is defined as the ratio of the total volume of pores to the total volume of the ROI. Since the connected pores have an important effect on the permeability of cement-based materials, the classification of the connected pores and the closed pores have been done using Avizo software. The connected pores (yellow parts in Fig.s 4c, 4f, 4i and 4 l) are defined as the pores connected to any boundary of the ROI. The closed pores (red parts in Fig.s 4c, 4f, 4i and 4 l) are defined as the pores that has no contact with any face of the ROI. The use of the ROI to define the sample boundaries is a kind of subjective and may overcount the connected pores for a real sample. This point is addressed below.

Since the size of the 3D rendered volume image is 18 μm × 33 μm × 33 μm, the total calculated volume of the pores is 2744 μm^3, the porosity of the measured sample hydrated for 7 days is 14.1%. The connected pores and the closed pores count 6.2% and 7.9%. The evolution of the porosity at various ages is shown in Fig. 5b and c. The results are consistent with that of Gallucci[17] with CT measurement that total porosity and the average radius of pores of hardened cement paste decrease over time. The poor connectivity of pores at longer curing time was also confirmed by Promentilla[40,41] with CT measurement.

3.2.3. Region of interest (ROI)

In order to minimize the edge effect and reduce the time of data processing, the analyzed ROI in this study were chosen from the central region of the embedded hardened C_3S paste, where the homogeneity of the pastes is also considered as the best.[17] To verify whether the sampling is representative, the changes of the degree of hydration and porosity of the samples as a function of the selected ROI are shown in Fig. 6. In Fig. 6a, it can be seen that once the selected ROI are larger than

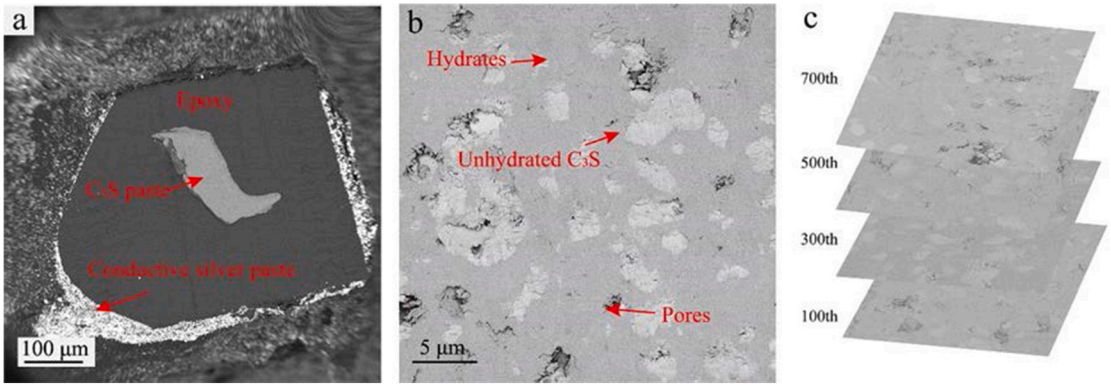

Fig. 3. Two-dimensional (2D) slice images of the hardened C_3S paste after 7 days of hydration from SBFSEM measurement. (a) BSE image of the whole sample. (b) The first acquired 2D image of the serial slices. (c) The 100th, 300th, 500th and 700th images of the serial slices.

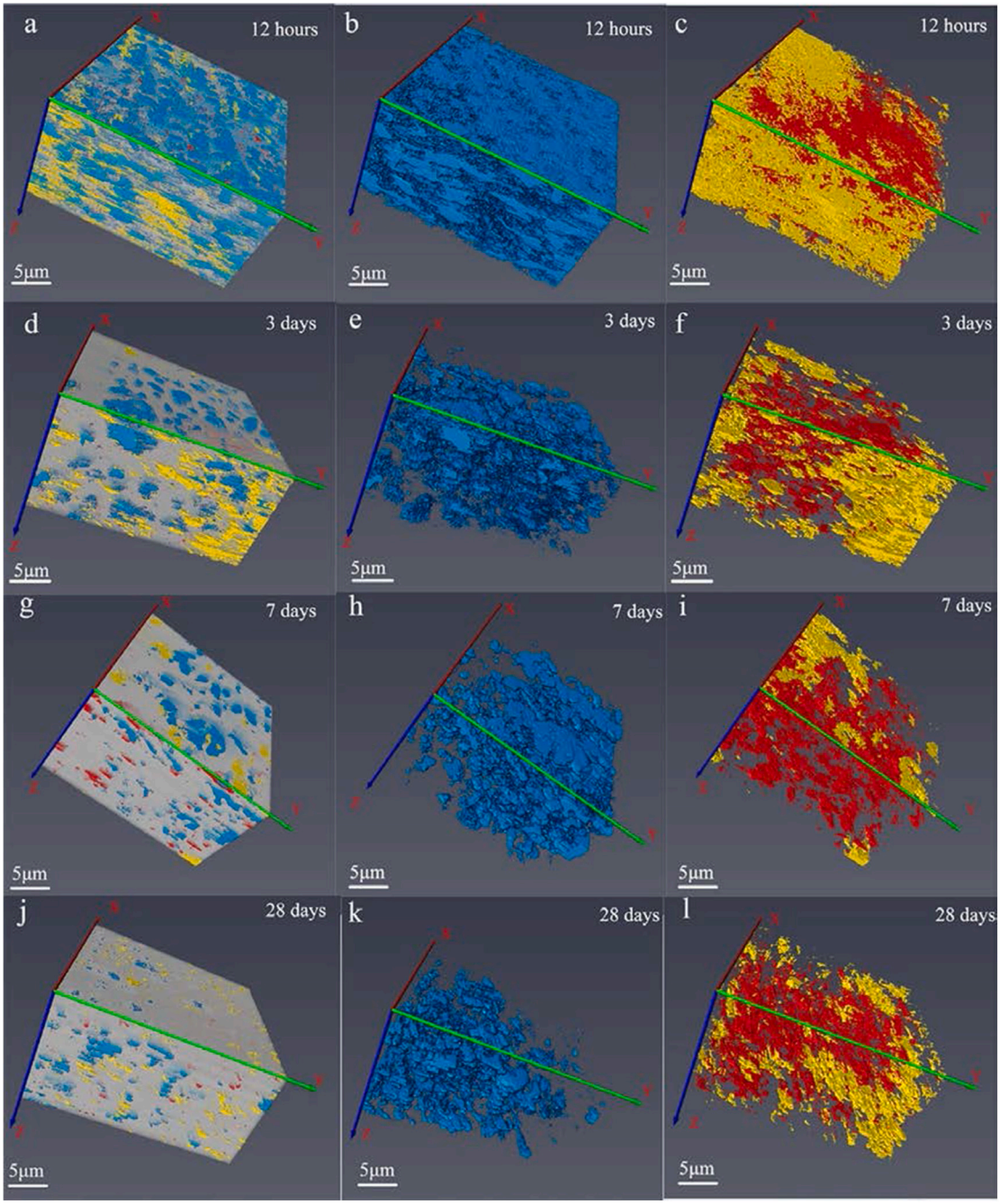

Fig. 4. 3D rendering images of the hardened C_3S pastes hydrated for various ages from SBFSEM measurement. (a) The hardened C_3S paste hydrated for 12 h. (b) The unhydrated C_3S particles (blue) and (c) The connected pores (yellow) and the closed pores (red) of the hardened C_3S paste hydrated for 12 h. (d) The hardened C_3S paste hydrated for 3 days. (e) The unhydrated C_3S particles (blue) and (f) the connected pores (yellow) and the closed pores (red) of the hardened C_3S paste hydrated for 3 days. (g) The hardened C_3S paste hydrated for 7 days. (h) The unhydrated C_3S particles (blue) and (i) the connected pores (yellow) and the closed pores (red) of the C_3S paste hydrated for 7 days. (j) The hardened C_3S paste hydrated for 28 days. (k) The unhydrated C_3S particles (blue) and (l) the connected pores (yellow) and the closed pores (red) of the C_3S paste hydrated for 28 days. (For interpretation of the references to colour in this figure legend, the reader is referred to the web version of this article.)

1.4×10^4 μm^3, their calculated hydration degrees tend to be stable. The calculated porosity of the samples tends to be stable after the selected ROI are larger than 1.8×10^4 μm^3 (Fig. 6b). This confirms that the selected ROI of (2.0×10^4) μm^3 in this work is appropriate.

3.3. Accuracy of SBFSEM

To verify the SBFSEM results, the degree of hydration and porosity of the hardened C_3S paste at 7 days from SBFSEM was compared with the results from TG-DSC (Fig. 7a) and MIP (Fig. 7b).

3.3.1. Comparison with TG-DSC measurements

The TG-DSC curves of the hardened C_3S paste hydrated for 7 days and 360 days are shown in Fig. 7a.

The degree of hydration of C_3S is determined by the ratio of the generated CH content at time t to the CH content in its fully hydrated status, as presented in Eq. (3).[42,43] $W(CH)_t$ refers to the mass of CH at time t, $W(CH)_\infty$ refers to the mass of CH produced when C_3S is fully

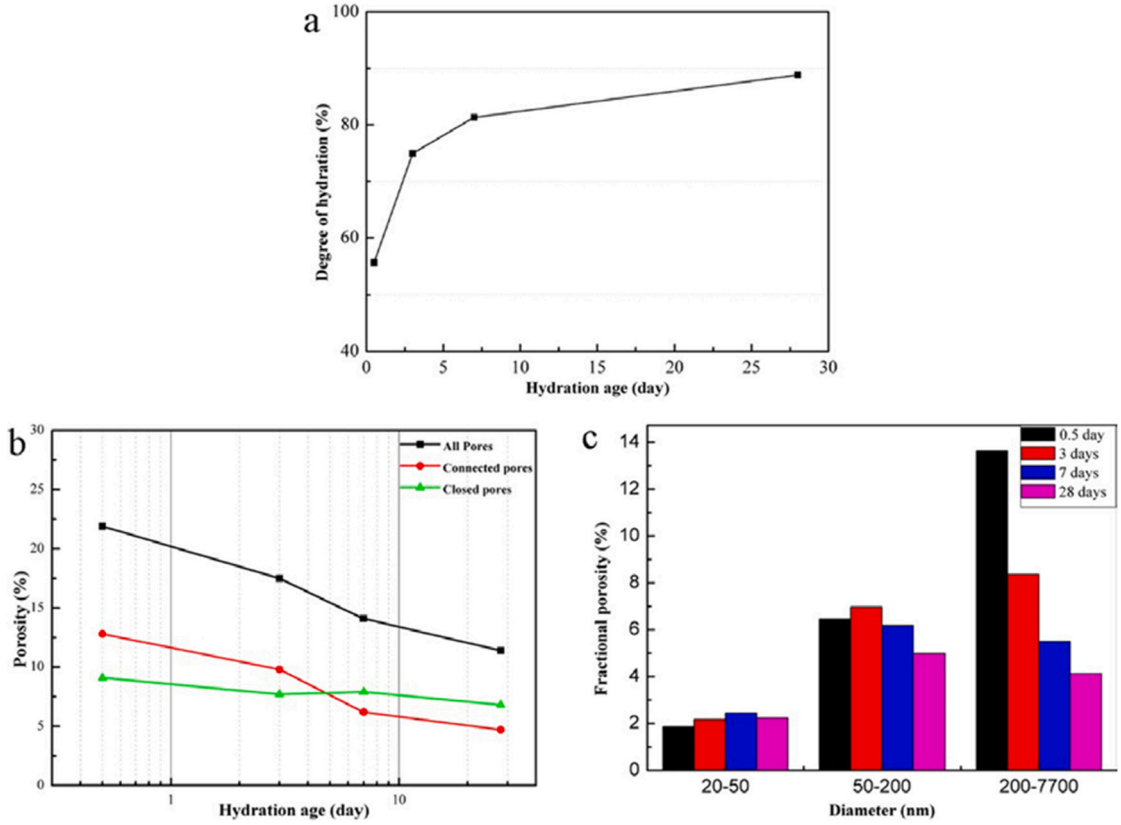

Fig. 5. Evolution of the degree of hydration and porosity of the C_3S pastes hydrated for 12 h, 3 days, 7 days and 28 days for a sample with w/c = 0.60. (a) The evolution of the degree of hydration during C_3S hydration. (b)The evolution of the total porosity, the porosity fractions of the connected and the closed pores during C_3S hydration. (c) The evolution of the porosity fractions of the pores with different sizes during C_3S hydration.

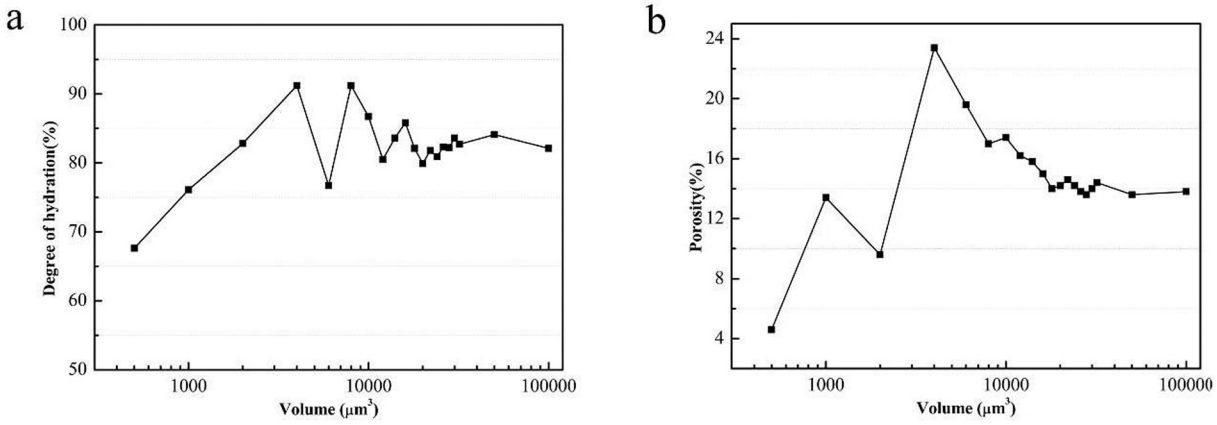

Fig. 6. Variation of the degree of hydration (a) and porosity (b) with selected ROI.

hydrated.

$$\text{Degree of Hydration } (\%) = \frac{W(\text{CH})_t}{W(\text{CH})_\infty} \times 100\% \quad (3)$$

The amount of CH generated during the C_3S hydration can be calculated according to Eq. (4) by the tangent method.[44,45]

$$\text{CH content } (\%) = \frac{\text{molar mass of CH}}{\text{molar mass of } H_2O} \times \text{CH mass loss } (\%) \quad (4)$$

The degree of hydration of the C_3S paste after 7 days of hydration calculated from TG-DSC results is 76.5%. This is slightly lower than the 81.3% obtained from the SBFSEM measurement. The possible reason is, in the 3D image segmentation process, some of the unhydrated particles with sizes around or smaller than 16.6 × 16.6 × 20 nm^3 (a voxel size of the acquired 3D SBFSEM image) were identified as the hydrates, which caused the degree of hydration from the SBFSEM measurement to be higher.

3.3.2. Comparison with MIP measurements

The pore size distribution of the sample after 7 days of hydration was measured by MIP as well, and the result is shown in Fig. 7b. There are two distinct peaks around the sizes of 15 nm and 200 nm. The porosity obtained by MIP is shown in Table 1. The total porosity is 21.4%. With reference to Wu's classification[46] of the pores of cement-based

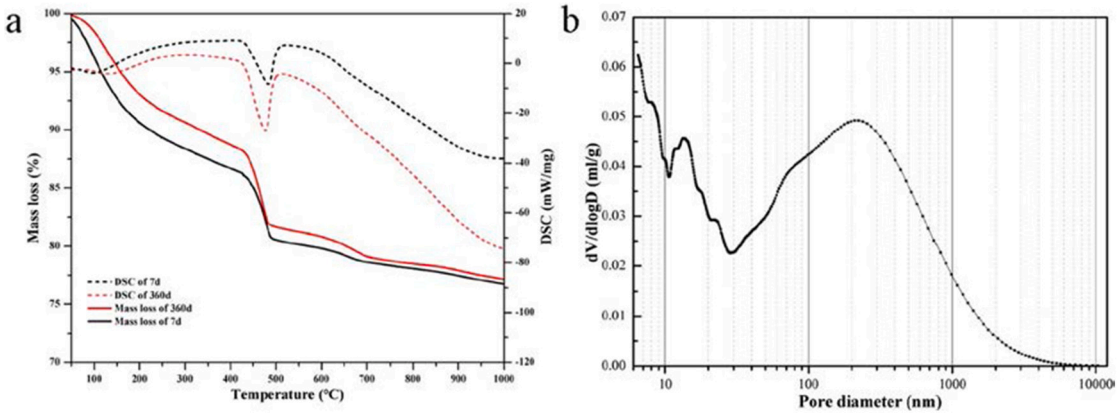

Fig. 7. The TG-DSC curves and pore size distribution of the hardened C_3S paste. (a)The TG-DSC curves of the C_3S paste hydrated for 7 days and 360 days. (b) The pore size distribution (dV/dlogD) of the hardened C_3S paste hydrated for 7 days.

Table 1
Porosity measured by MIP and SBFSEM.

Methods	Porosity (%)				
	Total	<20 nm	20 nm–50 nm	50 nm–200 nm	>200 nm
MIP	21.4	7.4	2.3	5.4	6.3
SBFSEM	14.1	–	2.4	6.2	5.5

materials, the porosity obtained by the MIP and SBFSEM measurements was classified and compared in Table 1. It should be noted that the two measurements were not performed using the same region of interest (ROI) of the same sample. Due to the intrinsic heterogeneity of the cement-based sample, the analytical data obtained by the two methods will have a certain extent of volatility. Pores smaller than 20 nm were not identified by SBFSEM due to the cutting thickness of the sample and the limitation of the resolution, which greatly reduced the measured total porosity from SBFSEM. For pore diameters in the range of 20 nm - 50 nm, the values obtained by the SBFSEM measurement (2.4%) is in good agreement with the 2.3% obtained by MIP. For pore diameters in the range of 50 nm - 200 nm, the porosity measured by SBFSEM (6.2%) is slightly higher than the 5.4% porosity obtained by MIP. This should be because MIP can only detect the connected pores, while SBFSEM measures both the connected and closed pores. For pores with diameters larger than 200 nm, the porosity of 5.5% obtained from SBFSEM is lower than that of 6.3% from MIP. The maximum pore diameter measured by the SBFSEM measurement is 7.7 μm, limited by the size of the measured sample. While the MIP measurement shows the largest pore is 10.4 μm. It is also possible that the high-pressure mercury intrusion causes the pores to be broken and enlarged during the measurement.

The SBFSEM measurement can visualize both the tortuosity and connectivity of the pores in three dimensions and can also detect the closed pores. Generally, the statistical results presented here (in Table 1) show that SBFSEM measurement agrees well with the classical MIP method.

3.4. Spatial structure development of the hardened C_3S pastes by SBFSEM

The 3D rendering of the SBFSEM results of the hardened C_3S pastes at various ages are shown in Fig. 4, in which the hydrates are rendered as grey, the unhydrated C_3S particles as blue and the pores as red and yellow. It can be seen that, as the hydration times increasing, the volumes of the unhydrated C_3S particles decrease. As shown in Fig. 5a, the degree of hydration of C_3S increase quickly before 7 days of hydration and slows down afterwards, indicating that C_3S has high reactivity with water.

From Fig.s 4c, 4f, 4i and 4 l, it can be seen that the volumes of total pores (yellow and red) and the connected pores (yellow) show a decreasing trend with the increase of the hydration ages, especially before 7 days, while the fluctuation of volumes of the closed pores (red) is small. This indicates that, the volume of the connected pores decreases faster than that of the closed pores while hydration is going on.

The changes of the total porosity, the porosity fractions of the connected pores and the closed pores are shown in Fig. 5b. The volumes of the closed pores in the hardened C_3S pastes decrease very slow, much slower than that of the connected pores, keep almost unchanged. This is because the hydration reaction occurs while the C_3S is in contact with water, hence the precipitated solid hydration products would occupy the spaces in the connected pores and the open regions. The needle-like C–S–H grows into the pore space, leading to very small water-filled capillary pores from quite young ages.[47] This leads to the decrease of the volumes of the connected pores. Additionally, some of the connected pores, especially small capillary pores, would evolve gradually into closed pores with the filling of hydrates into the pores during hydration, which further decreases the volumes of the connected pores and increase the volumes of the closed pores. On the other hand, the newly formed closed pores from connected pores may enwrap some free water hence hydration will continue in those closed pores. However, without continuous supply of water, the hydration inside the closed pores is limited, which makes the volumes of the closed pores decrease very slowly. Fig. 5c shows the porosity fractions of the pores with different sizes of the hardened C_3S pastes hydrated for 12 h, 3 days, 7 days and 28 days. It can be seen that the porosity fractions of the largest pores with diameters between 200 nm - 7700 nm decrease sharply during hydration, while smaller ones between 50 nm - 200 nm increase before 3 days of hydration and then decrease afterwards, and the smallest ones between 20 nm - 50 nm slightly increase before 7 days and decrease at 28 days. It demonstrates that, with the continued hydration, hydrates fill in the connected pores and hence separate the large pores into smaller ones, which causes the decrease of large pores all the way and the increase of smaller pores over a certain period of time, hence brings a finer pore structure and lower total porosity in the hardened C_3S paste. On the other hand, as seen in Fig.s 4c, 4f, 4i and 4 l visually, the largest pores are almost all connected pores and the smallest pores are mostly closed pores. As shown in Fig. 5c, the volume of the former group decreases fast and contributes to the increase of that of the latter by involving in the hydration reaction strongly, while the latter group involves in the hydration reaction much less.

4. Conclusions

In this work, the SBFSEM method is demonstrated to be a very promising 3D visualization technique at nano-scale for both imaging and quantitative study of the spatial structure of the hardened C_3S pastes

during hydration.

Evaluation of the degree of hydration and porosity of the selected different volumes of the ROI indicates that a volume of sample no less than 1.8×10^4 μm^3 needs to be used for 3D nano-structure investigation on the hydrated pure cement specimens.

The spatial distribution of the unhydrated C_3S particles, the hydrates and the pores in the hardened C_3S pastes were revealed directly in three dimensions at nano-scale with a voxel size of 16.6 nm × 16.6 nm × 20 nm. The degree of hydration based on the total volumes of the unhydrated C_3S particles was calculated. The pore structure of the hardened C_3S pastes was clearly revealed in three dimensions through SBFSEM measurements. The spatial tortuosity and connectivity information of the pores are visually presented. With the increase of hydration time, the connected pores in hardened C_3S paste decrease much faster than the closed pores. The porosity fractions of the large pores between 200 nm −7700 nm decreases steadily during hydration, while those between 20 nm - 200 nm increases firstly and then decreases, resulting in a denser hardened microstructure. It indicates that the formation of the pore network is a complex procedure which includes not only the partition of the open pores but also the formation of the new open and closed pores during hydration.

Materials availability

All the data related to the paper are provided in the main manuscript and the supplementary materials. Additional data related to this paper may be available from the correspondence authors upon reasonable requests.

Declaration of Competing Interest

The authors declare no conflict of financial interests.

Acknowledgements

This work was supported by the High-Level Talent Program “Materials Nano-structure” of Tongji University with grant No.s [152221] and [152243], the National Natural Science Foundation of China with grant No.s [51102181] and [U1534207]. B.C. thanks the support by the “Shanghai PuJiang Talent Program” with grant No. [18PJ1410400].

Appendix A. Supplementary data

Supplementary data to this article can be found online at https://doi.org/10.1016/j.matchar.2021.110973.

References

[1] K. Mei, X. Cheng, H. Zhang, Y. Yu, X. Gao, F. Zhao, J. Zhuang, X. Guo, The coupled reaction and crystal growth mechanism of tricalcium silicate (C_3S): an experimental study for carbon dioxide geo-sequestration wells, Constr. Build. Mater. 187 (2018) 1286–1294.
[2] Q. Hu, M. Aboustait, T. Kim, M.T. Ley, J.W. Bullard, G. Scherer, J.C. Hanan, V. Rose, R. Winarski, J. Gelb, Direct measurements of 3D structure, chemistry and mass density during the induction period of C_3S hydration, Cem. Concr. Res. 89 (2016) 14–26.
[3] A. De La Torre, S. Bruque, J. Campo, M. Aranda, The superstructure of C_3S from synchrotron and neutron powder diffraction and its role in quantitative phase analyses, Cem. Concr. Res. 32 (9) (2002) 1347–1356.
[4] L. Nicoleau, A. Nonat, A new view on the kinetics of tricalcium silicate hydration, Cem. Concr. Res. 86 (2016) 1–11.
[5] Y. Xi, D. Siemer, B. Scheetz, Strength development, hydration reaction and pore structure of autoclaved slag cement with added silica fume, Cem. Concr. Res. 27 (1) (1997) 75–82.
[6] K.L. Scrivener, A. Nonat, Hydration of cementitious materials, present and future, Cem. Concr. Res. 41 (7) (2011) 651–665.
[7] Y. Wei, W. Yao, X. Xing, M. Wu, Quantitative evaluation of hydrated cement modified by silica fume using QXRD, 27Al MAS NMR, TG–DSC and selective dissolution techniques, Constr. Build. Mater. 36 (2012) 925–932.
[8] R. Cook, K. Hover, Mercury porosimetry of hardened cement pastes, Cem. Concr. Res. 29 (6) (1999) 933–943.
[9] K.O. Kjellsen, H. Justnes, Revisiting the microstructure of hydrated tricalcium silicate—a comparison to Portland cement, Cem. Concr. Compos. 26 (8) (2004) 947–956.
[10] J.E. Rossen, K.L. Scrivener, Optimization of SEM-EDS to determine the C–A–S–H composition in matured cement paste samples, Mater. Charact. 123 (2017) 294–306.
[11] C.C. Yang, On the relationship between pore structure and chloride diffusivity from accelerated chloride migration test in cement-based materials, Cem. Concr. Res. 36 (7) (2006) 1304–1311.
[12] Y. Su, J. Feng, P. Jin, C. Qian, Influence of bacterial self-healing agent on early age performance of cement-based materials, Constr. Build. Mater. 218 (2019) 224–234.
[13] S. Wang, X. Ma, L. He, Z. Zhang, L. Li, Y. Li, High strength inorganic-organic polymer composites (IOPC) manufactured by mold pressing of geopolymers, Constr. Build. Mater. 198 (2019) 501–511.
[14] Q. Ren, Z. Zeng, Z. Jiang, Q. Chen, Incorporation of bamboo charcoal for cement-based humidity adsorption material, Constr. Build. Mater. 215 (2019) 244–251.
[15] A.J. Allen, J.J. Thomas, Analysis of C–S–H gel and cement paste by small-angle neutron scattering, Cem. Concr. Res. 37 (3) (2007) 319–324.
[16] H. Zhao, D. David, Quantitative backscattered electron analysis of cement paste, Cem. Concr. Res. 22 (4) (1992) 695–706.
[17] E. Gallucci, K. Scrivener, A. Groso, M. Stampanoni, G. Margaritondo, 3D experimental investigation of the microstructure of cement pastes using synchrotron X-ray microtomography (μCT), Cem. Concr. Res. 37 (3) (2007) 360–368.
[18] M. Moradian, Q. Hu, M. Aboustait, M.T. Ley, J.C. Hanan, X. Xiao, G.W. Scherer, Z. Zhang, Direct observation of void evolution during cement hydration, Mater. Design 136 (2017) 137–149.
[19] S.B. Xue, P. Zhang, J.W. Bao, L.F. He, Y. Hu, S.D. Yang, Comparison of mercury intrusion porosimetry and multi-scale X-ray CT on characterizing the microstructure of heat-treated cement mortar, Mater. Charact. 160 (2020) 110085.
[20] S. Brisard, M. Serdar, P.J.M. Monteiro, Multiscale X-ray tomography of cementitious materials: a review, Cem. Concr. Res. 128 (2020) 105824.
[21] B. Chen, W. Lin, X.P. Liu, F. Iacoviello, P. Shearing, I. Robinson, Pore structure development during hydration of Tricalcium silicate by X-ray Nano-imaging in three dimensions, Constr. Build. Mater. 200 (2019) 318–323.
[22] W. Denk, H. Horstmann, Serial block-face scanning electron microscopy to reconstruct three-dimensional tissue nanostructure, PLoS Biol. 2 (11) (2004), e329.
[23] B. Chen, M. Yusuf, T. Hashimoto, A.K. Estandarte, G. Thompson, I. Robinson, Three-dimensional positioning and structure of chromosomes in a human prophase nucleus, Sci. Adv. 3 (7) (2017), e1602231.
[24] H. Reingruber, A. Zankel, C. Mayrhofer, P. Poelt, Quantitative characterization of microfiltration membranes by 3D reconstruction, J. Membrane Sci. 372 (1–2) (2011) 66–74.
[25] V. Ageh, D. Choudhuri, T.W. Scharf, High frequency reciprocating sliding wear behavior and mechanisms of quaternary metal oxide coatings, Wear 330-331 (2015) 390–399.
[26] A. Trueman, S. Knight, J. Colwell, T. Hashimoto, J. Carr, P. Skeldon, G. Thompson, 3-D tomography by automated in situ block face ultramicrotome imaging using an FEG-SEM to study complex corrosion protective paint coatings, Corros. Sci. 75 (2013) 376–385.
[27] B. Chen, M. Guizar-Sicairos, G. Xiong, L. Shemilt, A. Diaz, J. Nutter, N. Burdet, S. Huo, J. Mancuso, A. Monteith, F. Vergeer, A. Burgess, I. Robinson, Three-dimensional structure analysis and percolation properties of a barrier marine coating, Sci. Rep. 3 (2013) 1177.
[28] S. Busse, T. Hornschemeyer, C. Fischer, Three-dimensional reconstruction on cell level: case study elucidates the ultrastructure of the spinning apparatus of Embia sp. (Insecta: Embioptera), Roy. Soc. Open Sci. 3 (10) (2016) 160563.
[29] K. Mukherjee, H.R. Clark, V. Chavan, E.K. Benson, G.J. Kidd, S. Srivastava, Analysis of brain mitochondria using serial block-face scanning electron microscopy, Jove-J. Vis. Exp 113 (2016) e54214.
[30] K. Kjellsen, B. Lagerblad, Microstructure of tricalcium silicate and Portland cement systems at middle periods of hydration-development of Hadley grains, Cem. Concr. Res. 37 (1) (2007) 13–20.
[31] C.A. Schneider, W.S. Rasband, K.W. Eliceiri, NIH image to ImageJ: 25 years of image analysis, Nat. Methods 9 (7) (2012) 671–675.
[32] S. Borrett, L. Hughes, Reporting methods for processing and analysis of data from serial block face scanning electron microscopy, J. Microsc-Oxford 263 (1) (2016) 3–9.
[33] J. Zhang, G.W. Scherer, Comparison of methods for arresting hydration of cement, Cem. Concr. Res. 41 (10) (2011) 1024–1036.
[34] Y. Liu, H.E. King, M.A. van Huis, M.R. Drury, O. Plümper, Nano-tomography of porous geological materials using focused ion beam-scanning electron microscopy, Minerals 6 (4) (2016).
[35] M.B. Bird, S.L. Butler, C.D. Hawkes, T. Kotzer, Numerical modeling of fluid and electrical currents through geometries based on synchrotron X-ray tomographic images of reservoir rocks using Avizo and COMSOL, Comput. Geosci. 73 (2014) 6–16.
[36] K.L. Scrivener, The use of backscattered electron microscopy and image analysis to study the porosity of cement paste, Mater. Res. Soc. Symp. Proc. 137 (1989) 129.
[37] M.Z. Zhang, Y.J. He, G. Ye, D.A. Lange, K. van Breugel, Computaional investigation on mass diffusivity in Portland cement paste based on X-ray computed microtomography (μCT) image, Constr. Build. Mater. 27 (2012) 472–481.
[38] X. Feng, E.J. Garboczi, D.P. Bentz, P.E. Stutzman, T.O. Mason, Estimation of the degree of hydration of blended cement pastes by a scanning electron microscope point-counting procedure, Cem. Concr. Res. 34 (10) (2004) 1787–1793.

[39] J. Jain, N. Neithalath, Analysis of calcium leaching behavior of plain and modified cement pastes in pure water, Cem. Concr. Com. 31 (3) (2009) 176–185.
[40] M.A.B. Promentilla, T. Sugiyama, T. Hitomi, N. Takeda, Characterizing the 3D pore structure of hardened cement paste with synchrotron microtomography, J. Adv. Concr. Technol. 6 (2) (2008) 273–286.
[41] M.A.B. Promentilla, T. Sugiyama, T. Hitomi, N. Takeda, Quantification of tortuosity in hardened cement pastes using synchrotron-based X-ray computed microtomography, Cem. Concr. Res. 39 (6) (2009) 548–557.
[42] W. Sha, E. O'Neill, Z. Guo, Differential scanning calorimetry study of ordinary Portland cement, Cem. Concr. Res. 29 (9) (1999) 1487–1489.
[43] P. Mounanga, A Khelidj, A. Loukili, W. Baroghel-Bouny, predicting $Ca(OH)_2$ content and chemical shrinkage of hydrating cement pastes using analytical approach, Cem. Concr. Res. 32 (2) (2004) 255–265.
[44] X. Kang, X. Zhu, J. Qian, J. Liu, Y. Huang, Effect of graphene oxide (GO) on hydration of tricalcium silicate (C_3S), Constr. Build. Mater. 203 (2019) 514–524.
[45] H.G. Midgley, The determination of calcium hydroxide in set Portland cements☆, Cem. Concr. Res. 9 (1) (1979) 77–82.
[46] Z. Wu, H. Lian, High Performance Concrete[M], China Railway Publishing House, 1990.
[47] Q.H. Do, S. Bishnoi, K.L. Scrivener, Numerical simulation of porosity in cements, Trans. Porous. Med. 99 (1) (2013) 101–117.